

THE NEW LONG-PERIOD AM HERCULIS SYSTEM RX J2157.5+0855

G. H. TOVMASSIAN

Observatorio Astronómico Nacional, Instituto de Astronomía, Universidad Nacional Autónoma de México, Mexico; gag@astrosen.unam.mx

J. GREINER AND A. D. SCHWOPE

Astrophysical Institute Potsdam, Potsdam, Germany

P. SZKODY¹

Department of Astronomy, University of Washington, Seattle, WA 98195

G. SCHMIDT

Steward Observatory, University of Arizona, Tucson, AZ 85721

F.-J. ZICKGRAF

Observatoire Astronomique de Strasbourg, France

A. SERRANO

Instituto Nacional de Astrofísica Óptica y Electrónica, AP 51 y 216, Puebla, Puebla, México

J. KRAUTTER AND I. THIERING

Landessternwarte Königstuhl, 69117 Heidelberg, Germany

AND

S. V. ZHARIKOV²

Special Astronomical Observatory, 357147 Nizhnij Arkhyz, Russia

Received 1999 November 8; accepted 2000 February 17

ABSTRACT

The identification and study of the optical counterpart of the *ROSAT*-discovered AM Her system RX J2157.5+0855 is reported. We present high time-resolution spectrophotometric, spectropolarimetric, and multicolor CCD-photometric observations of this polar obtained when the system was actively accreting. The 3.375 hr orbital period of the system places it among a few long-period AM Her objects. The emission lines clearly reveal the presence of at least two different line components with different widths and radial velocity variations. The Balmer emission lines contain significant contribution from the X/UV-illuminated hemisphere of the secondary star. The H α line is deblended into two components, which we identify with the secondary star and the accretion stream. The circular polarization unambiguously confirms the magnetic nature of this newly discovered cataclysmic variable with ≈ 20 MG strength deduced by cyclotron emission modeling. Combining radial velocity and light curves with polarization variations provides additional information about the system geometry.

Subject headings: accretion, accretion disks — binaries: eclipsing — novae, cataclysmic variables — stars: individual (RX J2157.5+0855) — stars: magnetic fields — X-rays: stars

1. INTRODUCTION

Cataclysmic variables (CVs) are close binary systems, in which a compact white dwarf (WD) primary accretes matter from a Roche lobe-filling late-type main-sequence secondary component. AM Her systems, or polars, are a subclass of cataclysmic variables where the magnetic field of the white dwarf is strong enough to channel the accretion along the magnetic field lines, thus preventing the formation of an accretion disc and synchronizing the rotation of the white dwarf with the orbital period (Warner 1995). A region in the accretion column above the WD, which is formed as a result of a shock of accreting matter, gives rise to hard X-ray radiation (often described with a bremsstrahlung model) and polarized cyclotron radiation. In addition, a strong soft component of X-ray radiation has been frequently observed from polars; this is assumed to be a result of the heating of the WD and thus is usually modeled in terms of blackbody emission with 20–50 eV temperature.

Within a program devoted to the optical identification of a complete sample of northern *ROSAT* all-sky survey (RASS) X-ray sources, we identified a new magnetic cataclysmic variable. Since 1991 October nearly 800 X-ray sources have been observed within the identification program.³ A detailed description of the project is given by Zickgraf et al. (1997). Here we report the identification and detailed follow-up observations of the optical counterpart of the *ROSAT* all-sky survey X-ray source RX J2157.5+0855 (= 1RXS J215731.4+085458).

The RASS and follow-up optical identification of soft X-ray sources have led to the discovery of a large number of new AM Her binary systems (see summaries by Beuermann & Burwitz 1995, Schwöpe 1995, Beuermann 1997, and references therein). The increased number of objects improves the statistics for such parameters as orbital and spin periods, magnetic field strengths, spatial distribution, etc., thus helping to refine existing theoretical models and evolutionary hypotheses and/or providing observational evi-

¹ Observations reported here were obtained in part at the Apache Point Observatory 3.5 m telescope, which is owned and operated by the Astrophysical Research Consortium (ARC).

² Present address: Observatorio Astronómico Nacional, Instituto de Astronomía, Universidad Nacional Autónoma de México, Mexico.

³ The identification project is a collaboration of the Max-Planck-Institut für extraterrestrische Physik, Garching, Germany, the Landessternwarte Heidelberg (LSW), Germany, and the Instituto Nacional de Astrofísica, Óptica y Electrónica (INAOE), Puebla, Tonantzintla, Mexico.

dence of the systems with theoretically predicted physical parameters.

2. DATA ACQUISITION AND REDUCTION

2.1. X-Ray Observations

The sky area of RX J2157.5+0855 was scanned in the RASS during 1990 November 11–19 for a total exposure time of 315 s. RX J2157.5+0855 is found as a source with a total of 24 photons, which corresponds to a vignetting-corrected count rate of 0.076 ± 0.010 counts s^{-1} in the *ROSAT* PSPC. No strong variability in the X-ray intensity is seen within the statistical level. The spectrum as derived from these 24 photons is rather soft for *ROSAT* standards but certainly much harder than the majority of new polars found from *ROSAT* identifications. The standard *ROSAT* hardness ratio⁴ values are $HR1 = -0.44 \pm 0.24$ and $HR2 = 0.08 \pm 0.45$. A spectral fit, admittedly with very poor significance given the low number of photons, suggests no measurable absorption ($< 2 \times 10^{20}$ cm^{-2}), implying a rather low distance.

For a two-component (blackbody and thermal bremsstrahlung) spectral fit with adopted temperatures of 40 eV and 20 keV, respectively, the unabsorbed flux in the 0.1–2.4 keV range is 5.5×10^{-13} ergs cm^{-2} s^{-1} (and 1.1×10^{-12} ergs cm^{-2} s^{-1} bolometric), corresponding to a luminosity of 6.5×10^{29} (D/100 pc)² ergs s^{-1} . RX J2157.5+0855 has not been covered by any (serendipitous) *ROSAT* pointing, so the X-ray parameters cannot be improved further.

2.2. Optical Observations

The original identification observations were carried out at the 2.15 m telescope of the Guillermo Haro Observatory, which is operated by INAOE and is located near Cananea, Sonora, Mexico. For the purpose of the identification project the LSW has constructed an efficient faint object

⁴ HR1 is the normalized count difference $(N_{52-201} - N_{11-41}) / (N_{11-41} + N_{52-201})$, where N_{a-b} denotes the number of counts in the PSPC between channel a and channel b, and HR2 is similarly defined as $(N_{91-200} - N_{50-90}) / N_{50-200}$ with the count number divided by 100 corresponding roughly to the energy in keV.

spectrograph (Landessternwarte Faint Object Spectrograph and Camera [LFOSC]). It allows direct CCD imaging, filter photometry, and, in particular, multiobject spectroscopy by using interchangeable hole masks with circular holes in the focal plane of the telescope (Zickgraf et al. 1997).

After the primary identification, the optical counterpart was observed at the 2.1 m telescope of Observatorio Astronómico Nacional de San Pedro Mártir (OAN SPM) on various occasions between 1996 and 1998 (see Table 1). However, the faintness of the object and spectral resolution of 2.3 Å pixel⁻¹ reached with the Boller & Chivens (B&Ch) spectrograph was not enough to resolve details of the emission lines.

Therefore, 42 spectra of RX J2157.5+0855 were obtained during two half-nights (1/2 Sept. 1998) with the 3.5 m ARC telescope at Apache Point Observatory (APO) using the double imaging spectrograph (DIS) set in two wavelength regions, 4200–5100 and 5800–6850 Å, with spectral resolutions of 1.61 and 1.3 Å pixel⁻¹, respectively. This corresponds to an overall FWHM resolution of 3.0 and 2.4 Å in the corresponding bands. The optimal extraction method was applied within the IRAF⁵ long-slit spectral reduction package after standard preliminary procedures for CCD observations.

Three weeks later, spectropolarimetric data were acquired at the Multiple Mirror Telescope (MMT) of Steward Observatory. Data were acquired with the CCD Spectropolarimeter described by Schmidt, Stockman, & Smith (1992), utilizing a 1200 × 800 Loral CCD that is thinned and antireflection coated for enhanced quantum efficiency. In addition to providing circular or linear spectropolarimetry, low-resolution total flux spectra are obtained in a wide range from 4000 to 8000 Å. We chose to measure circular polarization of the radiation from the

⁵ IRAF is the Image Reduction and Analysis Facility, a general purpose software system for the reduction and analysis of astronomical data. IRAF is written and supported by the IRAF programming group at the National Optical Astronomy Observatories (NOAO) in Tucson, Arizona. NOAO is operated by the Association of Universities for Research in Astronomy (AURA), Inc., under cooperative agreement with the National Science Foundation

TABLE 1
LOG OF OPTICAL OBSERVATIONS

Date UT	JD	Telescope + Equipment	Filter/Wavelength	Duration (minutes)	Exposure (s)	Site
1996 Aug 11	2450306	2.1 m, B&Ch spectrograph	3600–6200	180	1200	SPM
1996 Aug 12	2450307	2.1 m, B&Ch spectrograph	4100–6700	80	1200	SPM
1996 Aug 13	2450308	2.1 m, B&Ch spectrograph	4100–6700	60	1200	SPM
1996 Aug 14	2450309	2.1 m, B&Ch spectrograph	4100–6700	180	1200	SPM
1996 Oct 09	2450366	1.0 m, CCD	B	200	600	SAO
1997 Aug 31	2450660	2.1 m, B&Ch spectrograph	4200–6800	60	1200	SPM
1997 Sep 01	2450661	2.1 m, B&Ch spectrograph	4200–6800	40	1200	SPM
1997 Sep 02	2450662	2.1 m, B&Ch spectrograph	4000–7800	100	1800	SPM
1998 Aug 18	2451043	1.5 m, CCD TEK2K	R	380	30	SPM
1998 Aug 19	2451044	1.5 m, CCD TEK2K	B	345	45	SPM
1998 Aug 31	2451056	3.5 m, DIS	4180–5000	430	515	APO
1998 Aug 31	2451056	3.5 m, DIS	5795–6835	430	515	APO
1998 Sep 01	2451057	3.5 m, DIS	4180–5000	60	515	APO
1998 Sep 01	2451057	3.5 m, DIS	5795–6835	60	515	APO
1998 Sep 23	2451079	MMT Spectro-Polarimeter	4000–8000	145	600	Steward Obs.

object. Fourteen spectra were obtained within a time span slightly less than the orbital period of RX J2157.5+0855 under very good sky conditions, making flux calibration very reliable.

We also acquired photometry at SPM using CCD direct imaging with broadband filters (B , R), following the object about 6 hr in each band. The 3 minutes individual exposures were deployed consecutively. The data were reduced using the IRAF DAOPHOT package. Simple differential photometry was applied by measuring the object's magnitude in comparison with the field stars of comparable magnitude. Multiple apertures were probed during the measurements. The optimal aperture size (usually only 30%–40% larger than FWHM) was chosen to yield the smallest rms produced, rather than fully integrating the radiation from the source. Thus, the precise magnitude of the object never was measured. However, by rough estimate the system flickers around 18.5 mag at high state, at which all our observations supposedly were carried out.

The combined log of all optical observations is presented in Table 1.

3. IDENTIFICATION AND POSITION

The initial direct imaging revealed the presence of two optical candidates brighter than $R = 23$ mag in the error circle of RX J2157.5+0855. Multiobject spectroscopy with a resolution of 18 \AA was performed on each of the candi-

dates on the same night. Inspection of the spectra showed the brightest object of the *ROSAT* 30" error box to be an emission-line object with spectral characteristics typical of cataclysmic variables.

Subsequent spectral observations carried out with the 2.1 m telescope of OAN SPM showed strong, broad emission lines of hydrogen, He I, and He II imposed on a blue continuum. We measured the position of the optical counterpart of RX J2157.5+0855 as (equinox 2000.0) R.A. = $21^{\text{h}}57^{\text{m}}32^{\text{s}}.3$, decl. = $08^{\circ}55'15'' (\pm 1'')$. Figure 1 shows a finding chart with the cataclysmic variable marked.

4. ANALYSIS AND RESULTS

4.1. Orbital Period

Although we have gathered a relatively large number of observations, estimation of the orbital period was not a straightforward task. This is due to the relatively long orbital period, coupled with the inhomogeneous data set available for this purpose (photometry, polarimetry, and spectroscopy). We determined the orbital period by Fourier methods using the radial velocities (RVs) of emission lines. The central wavelengths of the emission lines were measured by fitting a single Gaussian to the line profiles of the low-resolution MMT spectra while other spectra first have been degraded in dispersion to the same 4 \AA pixel^{-1} resolution as the MMT spectra. The Gaussian usually picks up the strongest feature in the emission line. Unfortunately,

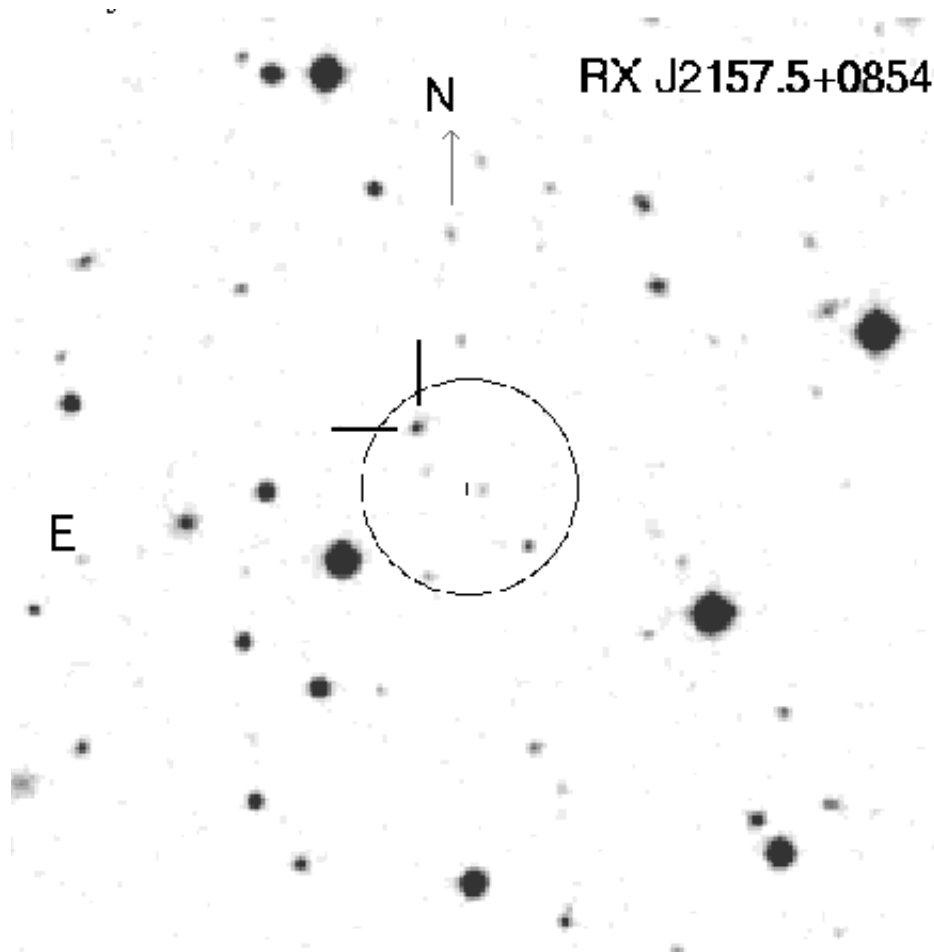


FIG. 1.—Identification chart showing the field of RX J2157.5+0855. The circle in the center shows the *ROSAT* 30" error box.

TABLE 2
MEASUREMENTS OF SPECTRAL LINES

Emission Line	Equivalent Width Range ^a (Å)	Flux Range ^a ($\times 10^{-14}$ ergs cm^{-2} s^{-1})	Relative Flux
H α	–80/–20	0.9/0.5	0.75
H β	–70/–20	1.2/0.67	1.0
H γ	–50/–30	1.6/0.8	1.33
He I λ 4471	–20/–8	0.54/0.2	0.45–0.3
He II λ 4686	–60/–15	0.8/0.4	0.6

^a The maximum and minimum measurements around an orbital period are presented.

the Balmer emission lines are composed of different components, with each component dominating at a different phase, so the resulting RV curve bears the signature of two waves and the power spectrum is contaminated with numerous aliases.

In addition, we used the light curves obtained from CCD photometry combined with measurements of the continuum flux in 40 Å bands in the blue and red parts of the spectra from all available spectroscopic observations. In Figure 2 the power spectrum of the light curve is presented comprising all data from photometric and spectroscopic observations.

The period estimate is sensitive to which lines were used or which continuum bands were included in the analysis. The values generally fall in the narrow range 0.14092–0.14002 days, confirming that there is most probably no discrepancy between photometric and spectroscopic periods. After checking most of the values by constraining phase-folded light curves and radial velocity curves we come to the conclusion that the best value based upon eye inspection is 0.14063 days \approx 3.375 hr. This coincides with

the strongest peak in the power spectrum obtained from the light curves (Fig. 2).

4.2. Spectroscopy: Emission-Line Components

In Figure 3 we show the sum of all high-resolution spectra from both blue and red channels. They exhibit strong Balmer emission lines, lines of neutral and ionized helium and of highly excited ions of C II and C III/N III. The appearance of the spectrum is typical of CVs. The flat Balmer decrement, the He II λ 4686 line strength comparable to that of H β , and the detection of the object as a soft X-ray source all suggest a magnetic CV caught in a high accretion state. The range of values for the total line fluxes and equivalent widths (EWs) of the major lines is presented in Table 2.

The emission-line profiles are smeared by summing and appear rather smooth in Figure 3. However, individual spectra show complicated, highly variable line profiles, characteristic of most magnetic CVs. These are better displayed in the trailed spectrogram presented in Figure 4. Three major lines are displayed here to demonstrate the presence of the two basic components found in polars.

In the first panel the He II line is shown at a scaling to highlight the presence of a large-amplitude wave, which

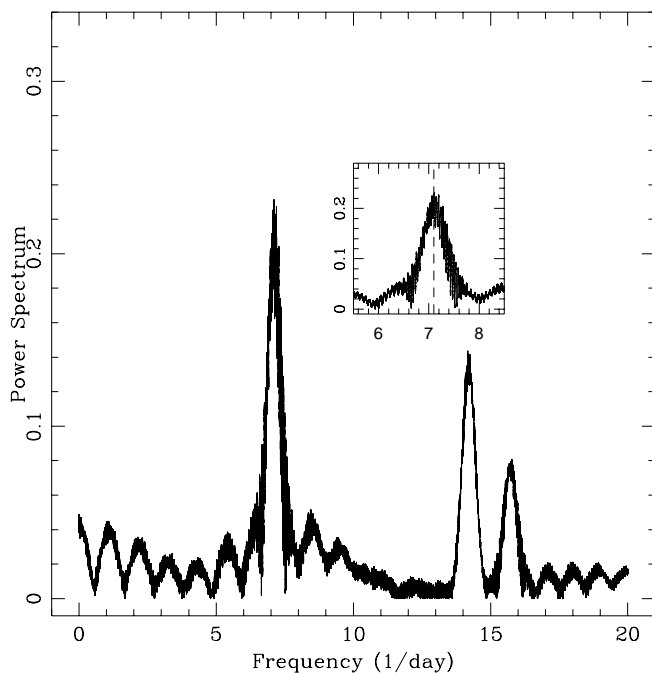


FIG. 2.—Power spectrum of the combined set of data with dominant peak corresponding to 0.14063 days orbital period. An expanded plot of the peak is shown in the inner frame with orbital period indicated by a vertical dashed line.

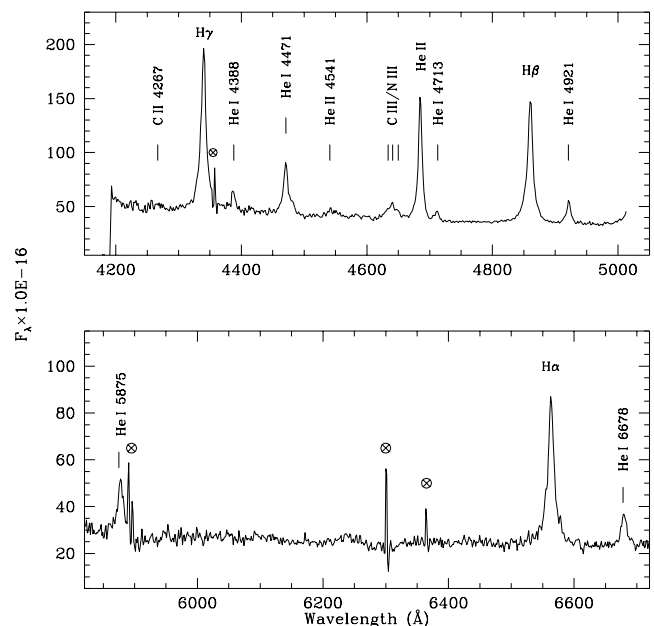


FIG. 3.—Sum of all high-resolution spectra of RX J2157.5+0855. Most of the lines are marked. The profiles are smoothed from co-adding.

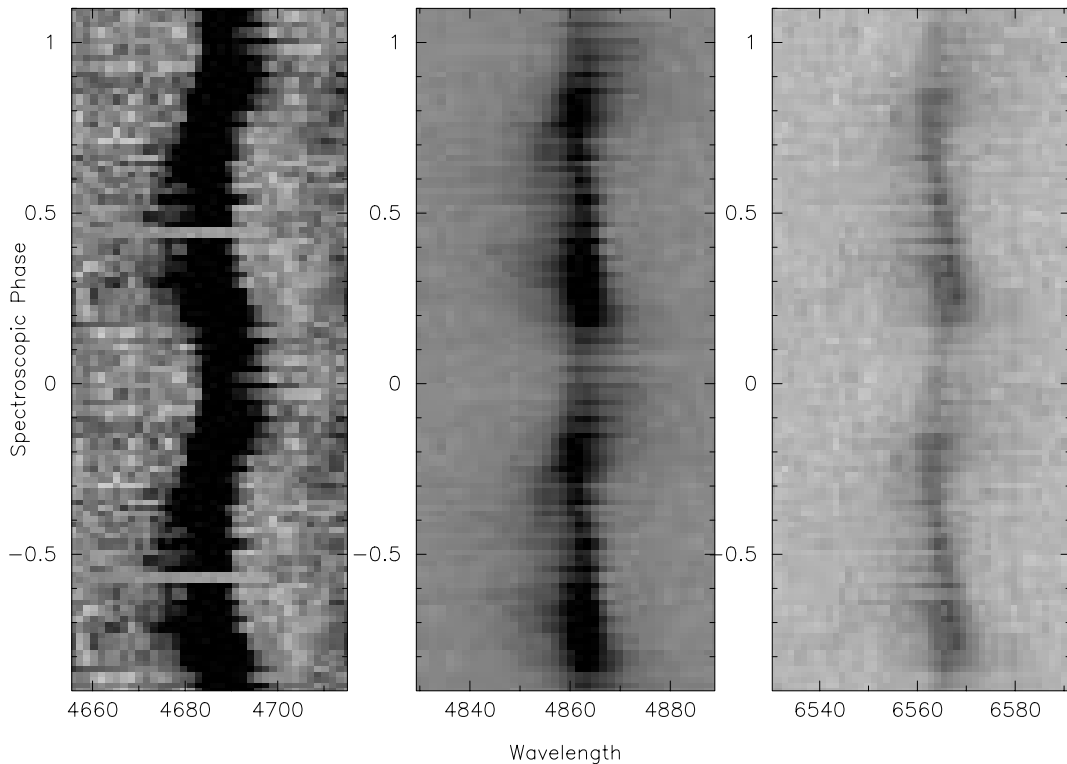


FIG. 4.—Trailed spectrogram of He II, H β , and H α lines. The gray scale is chosen in order to outline the narrow-line component in H α and high-velocity component in two other lines.

reaches maximum blueshift around phase 0.5 and maximum redshift around 0.0. Nevertheless, this component is broad, and one may note that the intensity around phase 0.5 suddenly decreases, making the component difficult to identify. The other component, less resolved on the first two panels, is better seen on the trailed spectra of H α presented on panel three. It is much stronger between phases 0.25 and 0.75 than on the other one-half of the orbit. Its maximum redshift is at $\phi = 0.75$, and it is much narrower and distinct where it could be detected. The pattern is identical to that of many other systems (i.e., Schwöpe, Mantel, & Horne 1997; Schwarz et al. 1998; Tovmassian et al. 1999), except probably that the former broad component, commonly called the high-velocity component (HVC), diminishes in phases of its maximum blueshift and that the latter component, called narrow emission line (NEL), is much sharper in the H α line profile than in He II. So, without much risk we can assume that, as in other cases, we see the NEL originating at the X-ray-irradiated side of the secondary and the HVC coming from the accretion stream.

Following the custom for other AM Her systems, the bright H β line was deconvolved with two Gaussians. The resulting components clearly fall into two categories as indicated by their widths, amplitudes of RV variations, and phases. The more easily distinguished NEL was first fitted with a sine curve with the previously determined orbital period $P_{\text{orb}} = 0.14063$ days. For a circular orbit the motion of the secondary star is described by

$$V_{\text{em}} = \gamma + K_2 \sin [2\pi(t - t_0)/P_{\text{orb}}], \quad (1)$$

where γ is the systematic velocity, K_2 is the projected velocity amplitude of the secondary star around the center of

mass, and t_0 is the time of blue-to-red zero crossing of the NEL radial velocities, corresponding to the inferior conjunction. Our best fit yielded $\gamma_{\text{NEL}} = 59 \text{ km s}^{-1}$, $K_{\text{NEL}} = 72 \text{ km s}^{-1}$ with a standard deviation of $\sigma = 21 \text{ km s}^{-1}$, and $t_0 = \text{HJD } 2,451,042.1898 \pm 0.002$.

The radial velocity behavior of the second, high-velocity component was estimated from fits to the residuals of the above deconvolution. We reached satisfactory fit to the line profiles in most cases, the exceptions lying mainly on the blue-to-red leg of the RV curve where the contribution from the irradiated secondary is minimal. Radial velocities of the HVC were also fitted by a sine curve, although large departures exist. The corresponding measurements and their fits are presented in Figure 5.

The rather modest RV semiamplitude of the HVC, 240 km s^{-1} , and the low amplitude of the narrow emission line component indicate that the inclination of RX J2157.5+0855 is relatively low.

In Figure 6 the fluxes and FWHM measurements of both components of H α are plotted. The mean width of the NEL component is 7 \AA , and its contribution is stronger at orbital phases $\phi = 0.2\text{--}0.8$. This is when the secondary faces the observer with its heated side. The width of NEL is actually much higher than one would expect from the models. This was seen also in HU Aqr by Schwöpe et al. (1997), where the NEL in H β and H γ was about 4 \AA wide, contrary to $2\text{--}2.5 \text{ \AA}$ for He II. This was explained as a result of optical thickness. A width of 7 \AA seems extreme. Unfortunately, the spectral resolution and the resolution of the components on the blue side of the spectrum were not good enough to let us compare NEL widths of different lines. The apparently large value of width may also be attributed to the underlying unresolved broad base component present in many

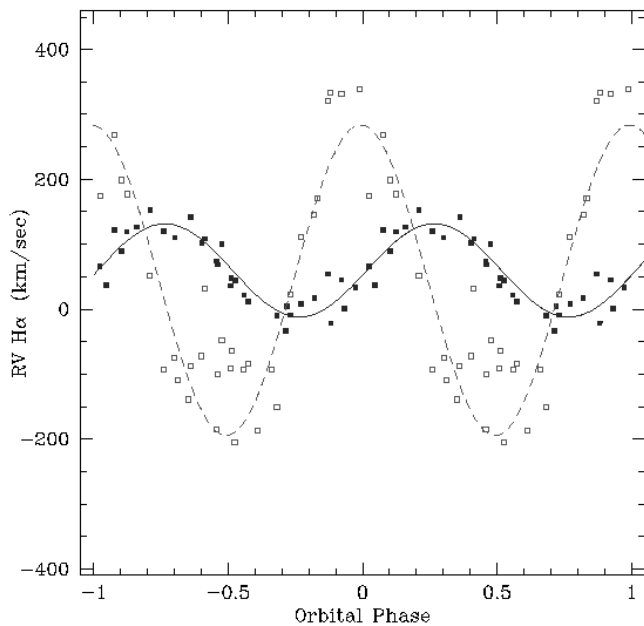


FIG. 5.—Radial velocity curves of the NEL and HV components of $H\alpha$. The solid line is a sine fit to the NEL radial velocities marked by filled points. The open points are RVs of the HVC. The dashed curve is the sine fit to them.

other similar systems and probably contaminating the NEL.

The broader HVC width ranges from 12 to 35 Å throughout the orbital period, and its strength clearly follows the changes in the continuum, which are described below.

Both components show a flux decrease at inferior conjunction of the secondary. Normally, the HVC flux is not expected to vary in parallel with the NEL, unless the accretion stream is aligned with the line of sight connecting both stars and either is occulted or polarized. The latter is not the

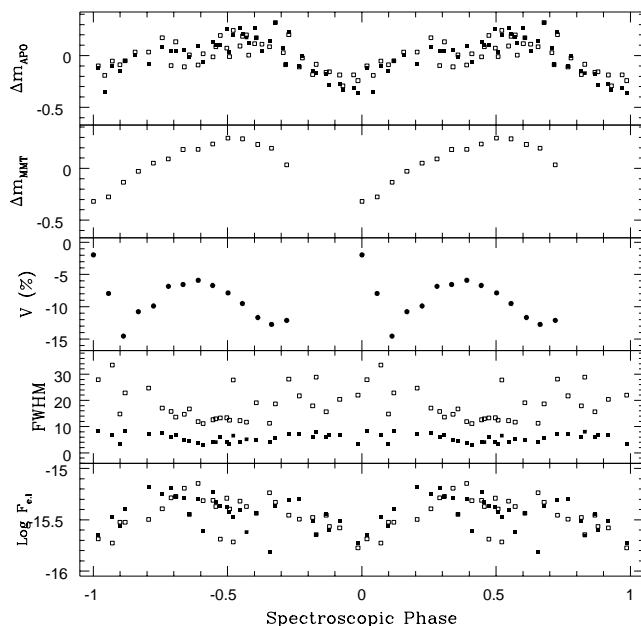


FIG. 6.—From bottom to top: (1) fluxes and (2) FWHM of the NEL (filled squares) and HV (open squares) components of $H\alpha$; (3) circular polarization; continuum flux in the narrow bands; open squares in the blue part and filled squares in the red part of spectra from low-resolution spectroscopy at (4) MMT and (5) APO.

case because we do not have any evidence of polarized line emission.

4.3. Spectroscopy: Doppler Tomography

In order to check the correct interpretation and phasing of the components, we performed Doppler tomography with the $He\ II$ and $H\beta$ lines using the filtered back-projection algorithm developed by Marsh & Horne (1988). The resulting Doppler maps are presented in Figure 7. The spot caused by the NEL is the dominant structure. It is located where the tip of the irradiated secondary should be. The Roche lobe of the secondary with $K_2 = 75\text{ km s}^{-1}$ and an arbitrary mass ratio $q = 0.5$ is drawn on the maps. Also shown is the accretion stream according to the above-mentioned parameters. However, the stream is less resolved on the tomograms. Apparently we see mostly the horizontal part on the maps, which corresponds to the ballistic part of the accretion stream. After coupling with the magnetic field it usually bends down on the maps toward negative V_y velocities. We examined Doppler maps of other magnetic CVs published in the literature observed with similar or better spectral and time resolution. We came to the conclusion that the low-inclination systems systematically show less intense and less resolved features of the accretion stream. Good examples of that may be seen in contributions by Schwöpe, Schwarz, & Staude (1999) and Hoard (1999). In that sense there is not much we can learn from Doppler tomography, and it is hardly possible to improve the numerical parameters of the system. However, we can affirm that the observed object is a diskless system with an irradiated secondary star with a K_2 velocity not exceeding the value as derived from the emission-line component separation.

4.4. Spectroscopy: Spectropolarimetry

Low-resolution spectropolarimetry revealed a high degree of circular polarization in RX J2157.5+0855, which was most prominent in the blue spectral regime. The wavelength-averaged circular polarization is plotted as a function of the orbital period in the third panel of Figure 6. In the same figure, the panel above shows the variability of the continuum flux in the corresponding spectra (wavelength average of the spectral flux in the interval 4750–4790 Å).

The first obvious thing to note is the high degree of polarization in RX J2157.5+0855, reaching 15% at phase 0.1. High circular polarization is extremely rare in astronomical objects. Among CVs only AM Her-type objects (polars) show circular polarization ranging up to 60% (Stockman et al. 1992). The observation of a large degree of circular polarization indicates the presence of a strong magnetic field. Two physically different processes might be contributing, either dichroism in the white dwarf photosphere or cyclotron radiation from the accretion plasma. The high degree and the phase dependence of the observed polarized radiation exclude the former possibility.

The photometric and polarization variability can be explained by a simple geometrical model assuming one accretion spot. The cyclotron radiation originating there is beamed into directions perpendicular to the local magnetic field (polar angle); i.e., maximum intensity is expected at a large polar angle. Such a view is realized in RX J2157.5+0855 at phase 0.4–0.5. At large polar angle cyclotron radiation V becomes circularly depolarized. The fact

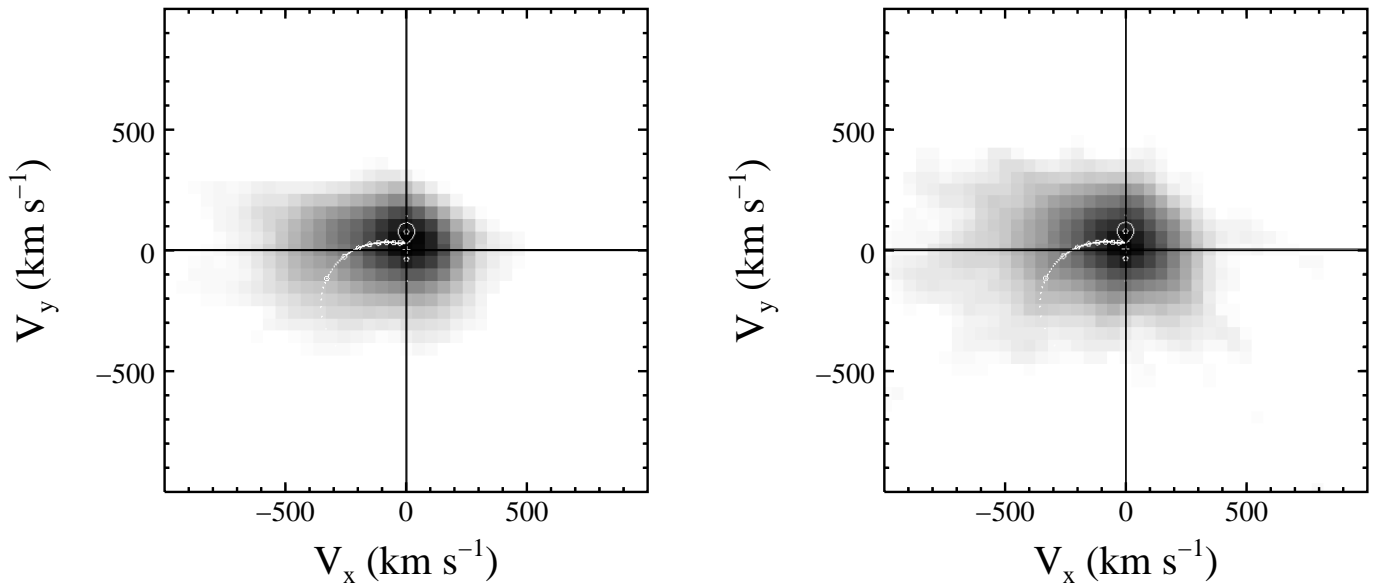


FIG. 7.—Doppler tomograms of (left) the He II emission line and (right) the H β emission line

that V does not reach zero at phase 0.4–0.5 means that the spot always remains in view of the observer and does not rotate over the limb of the white dwarf. Circular polarization is expected to reach its maximum at small polar angles ($\phi \simeq 0.9$ –1.0). Indeed, an increase of the degree of circular polarization is observed initially when the polar angle becomes smaller, but this increase is stopped abruptly in the phase interval 0.0–0.1. We interpret this drop in V as being caused mainly by depolarization due to background radiation components (accretion stream, photospheric radiation). Depolarization in the outer accretion stream might also contribute.

Several other polars show a very similar behavior of the circular polarization variation, among them MR Ser = PG 1550+191 (Liebert et al. 1982), V834 Cen (Schwope & Beuermann 1990), CP Tuc = AX J2315–592 (Ramsay et al. 1999), and AM Her, an archetype of the class itself (Latham, Liebert, & Steiner 1981).

We used the low-resolution flux spectra from spectropolarimetric observations to model the cyclotron emission and thus estimate the magnetic field strength of this polar. In order to separate the cyclotron spectrum from the other radiation components, we subtracted an average minimum spectrum ($\phi = 0.0$ –0.1) from the average spectrum at orbital maximum ($\phi = 0.5$ –0.6). This approach of separating the cyclotron component requires that the spectrum around phase zero be almost free of cyclotron radiation and that the underlying spectral components be not variable. The first assumption seems to be quite well fulfilled; the second is questionable since the emission lines are clearly variable. However, since our approach is the only possibility for separation of the spectral components, we proceed here using this difference spectrum. The difference spectrum is, apart from remaining emission lines, a smooth function peaking at about 5300 Å. The difference spectrum (as well as any of the individual spectra) does not show cyclotron harmonic emission, which would allow us to measure the field strength in the emitting plasma directly. The overall shape of the cyclotron spectrum resembles those of polars with intermediate field strength such as, e.g., MR Ser (24 MG) or V834 Cen (23 MG). In these two

systems weak cyclotron harmonics could be resolved in the high-accretion state. This might be suggestive of a somewhat lower field in RX J2157.5+0855.

For modeling the cyclotron spectrum of RX J2157.5+0855 we take the simplest view assuming a homogeneously emitting plasma. Cyclotron emission from such a plasma can be described by a characteristic temperature kT , the polar angle between the line of sight and the magnetic field θ , the field strength B , and a plasma parameter $\Lambda = ln_e/B$ (l : geometric size, n_e : electron density), which characterizes the optical thickness of the emitting volume (Wickramasinghe & Meggitt 1985). Assuming $kT = 20$ keV (a value of the order of the shock temperature) and $\theta = 80^\circ$ (a typical value for an accretion column with strong beaming), the observed wavelength of the cyclotron peak is reproduced with a field strength of 20 MG and a size parameter $\log \Lambda = 5.7$. Some of these quantities can be traded against each other. For example, lower values of B and T require higher values of Λ in order to shift the cyclotron peak to the observed value. The nondetection of cyclotron or Zeeman lines does not allow us to draw more definite conclusions about the plasma parameters with the present data set.

The suggested rather low value of the magnetic field strength is supported by the relatively hard X-ray spectrum typically found in low-field polars. It is also in agreement with the rather high value of the size parameter Λ (Beuermann & Burwitz 1995; Schwope 1996).

4.5. Photometry

The light curves obtained from the broadband photometry are presented in Figure 8. They resemble in great detail those of AM Her, the archetype of the class of magnetic CVs (see, e.g., Fig. 1 of Szkody & Brownlee 1977). The light curve shows broad (one-half orbital period wide), deep (up to 2 mag in R) persisting depressions. They are deeper and narrower in red. The broad minimum is perfectly centered at the phase $\phi = 0.0$ obtained from the spectroscopy.

Based on the polarimetry we conclude that the broad minimums occur when we look down at the magnetic pole, which is also the accretion pole and major contributor of

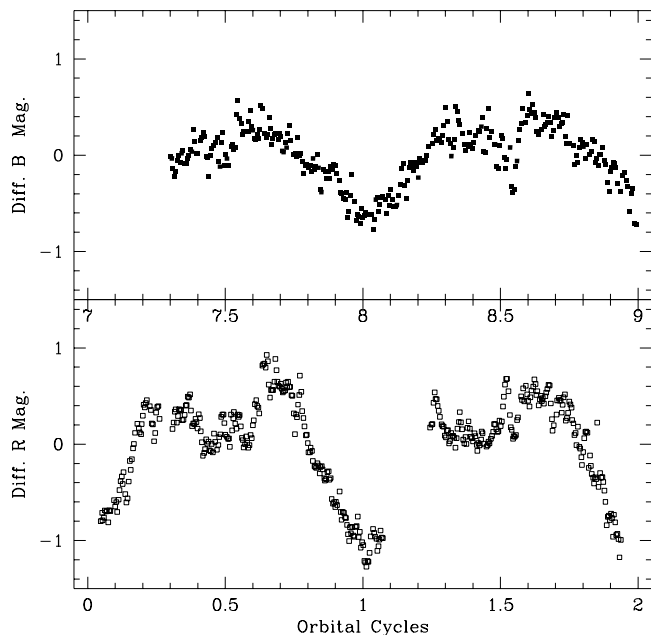


FIG. 8.—Light curves of RX J2157.5+0855 from *B* and *R* photometry

the system flux. Polarized emission escaping in a perpendicular direction to the magnetic lines fades as the system turns to a pole-on facing.

The explanation of the broad minimum as caused by polarized cyclotron emission finds additional support in the color dependence of the photometric light curve. The amplitude of variation is larger in the *R* band. There is about 0.1 phase lag between photometric minimum and the peak of the circular polarization; likewise, the photometric maximum is displaced about 0.1–0.15 phase relative to the minimum in polarization. These characteristic features were previously observed in MR Ser (Liebert et al. 1982).

Except this central feature, there is notable flickering especially pronounced in the *B* band. Furthermore, there is another broad but much shallower depression centered at phase 0.4 and at least one repeating narrow dip ($\phi = 0.51$) with varying amplitude. The flickering no doubt originates at the accretion spot; the narrow dip is probably evidence of curtaining of the accretion spot by the accretion stream.

4.6. The System Geometry

The newly discovered magnetic CV system shows familiar patterns of RV behavior, as well as photometric light curves and a circular polarization curve. Therefore, in analogy with other systems we can easily reconstruct a basic model of this object.

The optical emission of the system is dominated by cyclotron emission. Thus, since the cyclotron emission is beamed perpendicular to the field axis, the 2 mag photometric minimum could well be due to the fact that we look straight down to the magnetic pole while we look at a certain angle at other phases. Since the beaming is stronger at shorter wavelengths (higher harmonics), the minimum in the blue-band photometric light curve is broader than in the red. Its color dependence and symmetry are additional evidence in favor of the cyclotron-beaming model.

This interpretation is also consistent with the RVs because the high-velocity component is at maximum redshift, when the stream is flowing away from us, and at that moment the contribution of light from the funnel drops

nearly to zero because of the fanlike beaming of the cyclotron beams perpendicular to the magnetic field (Meggitt & Wickramasinghe 1982; Chanmugam & Dulk 1981). Meanwhile, the narrow, small-amplitude component coming from the companion star is in conjunction, just making the blue to red crossing.

Finally, the polarization behavior seems to be consistent with this picture: it rises toward photometric minimum and is lower at other phases. The absence of eclipses in the light curve of the system and the low amplitude of the NEL RV originating from the irradiated side of the secondary point to a low inclination angle of the orbital plane ($i < 75^\circ$). On the other hand, the difference in fluxes of the NEL at opposite phases and $K_2 \geq 75 \text{ km s}^{-1}$ shows that the inclination i cannot be much less than 40° – 50° . Combined with the fact that the polarization does not go back to zero for most of the phase, this implies that $\beta + i < 90^\circ$, where β is the colatitude of the magnetic field in the spot, which is not necessarily equal to (though $\pm 20^\circ$) the magnetic axis. On the other hand, the large photometric amplitude implies that the angle between the line of sight and the magnetic field varies over a large range. This implies that $\beta \sim i \sim 45^\circ$.

We did a rough estimate of the distance of the system, based on an assumed $m_R \approx 6 \times 10^{-17} \text{ ergs cm}^{-2} \text{ s}^{-1} = 18.7 \text{ mag}$ from flux-calibrated spectra and $A_v = 0.37 \text{ mag}$ in this direction. The latter is the total extinction in this direction, so even for a small distance of 100–200 pc, the system should suffer from this extinction. However, this number does not greatly affect the distance estimate. Our N_H constraint from the X-ray data is a 1σ value, so given the low statistics it is consistent with the assumption of 0.37 mag extinction value in deriving the distance estimate.

At the photometric minimum the contribution of the cyclotron radiation is minimal and a significant part of the flux should be coming from the secondary. The resulting distance could be 300–600 pc depending on whether we assume the spectral type of the secondary to be M4 or M5. Such a spectral type is consistent with the empirical relation established between orbital periods and the spectral types of secondaries in CVs (Patterson 1984). Any assumptions about the earlier spectral type of the secondary will push the distance to an unrealistic range for a CV.

5. SUMMARY

We have identified the *ROSAT* X-ray source RX J2157.5+0855 with a new magnetic cataclysmic variable (polar). The orbital period of the system is 0.14063 days $\approx 3.375 \text{ hr}$. Our observational data are not sufficient to determine whether the system is absolutely synchronous or not. However, the photometric period coincides with the spectroscopic one within 1 minute error over a 1 yr baseline. We regard the photometric period to be a spin period because the light-curve modulations are caused by cyclotron emission, while the spectral period is based on measurements of the narrow emission component coming from the irradiated secondary star that reflects the orbital motion of the system.

The combined photometric and polarimetric data unambiguously confirm the magnetic nature of the system. A magnetic field strength of 20 MG was derived from a simple model assuming a one-temperature plasma and a homogeneous one-value magnetic field. Furthermore, we conclude that the inclination of the system (i) and the colatitude of the magnetic axis (β) are about the same value of 45° .

A relatively low inclination of the system is supported by a corresponding low radial velocity (K_2) of the narrow emission component from the secondary star. We derived its 75 km s^{-1} value by using Gaussian deblending and Doppler tomography to separate this component within the emission lines. The radial velocity semi-amplitude of a component arising mainly from the ballistic part of the accretion flow is also much lower than in many other systems.

The authors acknowledge the participation of undergraduate students Ma.Hortensia Riesgo and Aixa Aubé

Cárdenas in some observations. G. T. is thankful to APO staff for hospitality and assistance during the observations. G. T. is supported by CONACYT under grant 25454-A. P. S. acknowledges partial support from NASA LTSA grant NAG-53345. J. G. is supported by the Deutsche Agentur für Raumfahrtangelegenheiten (DARA) GmbH under contract FKZ 50 QQ 9602 3. The *ROSAT* project is supported by the German Bundesministerium für Bildung, Wissenschaft, Forschung und Technologie (BMBF/DARA) and the Max-Planck-Society.

REFERENCES

- Beuermann, K. 1997, in High-Energy Astronomy and Astrophysics: Proc. Int. Colloq. on Perspectives of High-Energy Astronomy and Astrophysics, ed. P. Agrawal & P.R. Vishwanath (Hyderabad: University Press)
- Beuermann, K., & Burwitz, V. 1995, in ASP Conf. Ser. 85, Cape Workshop on Magnetic Cataclysmic Variables, ed. D. A. H. Buckley & B. Warner (San Francisco: ASP), 99
- Chanmugam, G., & Dulk, G. A. 1981, *ApJ*, 244, 569
- Hoard, D. W. 1999, in ASP Conf. Ser. 157, Annapolis Workshop on Magnetic Cataclysmic Variables, ed. C. Hellier & K. Mukai (San Francisco: ASP), 201
- Latham, D. W., Liebert, J., & Steiner, J. E. 1981, *ApJ*, 246, 919
- Liebert, J., Stockman, H. S., Williams, R. E., Tapia, S., Green, R. F., Rautenkranz, G., Ferguson, D., & Szkody, P. 1982, *ApJ*, 256, 594
- Marsh, T. R., & Horne, K. 1988, *MNRAS*, 235, 269
- Meggitt, S. M. A., & Wickramasinghe, D. 1982, *MNRAS*, 198, 71
- Patterson, J. 1984, *ApJS*, 54, 443
- Ramsay, G., Potter, S. B., Buckley, D. A. H., & Wheatley, P. J. 1999, *MNRAS*, 306, 809
- Schmidt, G. D., Stockman, H. S., & Smith, P. S. 1992, *ApJ*, 398, L57
- Schwarz, R., et al. 1998, *A&A*, 338, 465
- Schwöpe, A. D. 1995, *Rev. Mod. Astron.*, 8, 125
- . 1996, *Cataclysmic Variables and Related Objects*, ed. A. Evans & J. H. Wood (Dordrecht: Kluwer), 189
- Schwöpe, A. D., & Beuermann, K. 1990, *A&A*, 238, 173
- Schwöpe, A. D., Mantel, K.-H., & Horne, K. 1997, *A&A*, 319, 894
- Schwöpe, A. D., Schwarz, R., & Staude, A. 1999, in ASP Conf. Ser. 157, Annapolis Workshop on Magnetic Cataclysmic Variables, ed. C. Hellier & K. Mukai (San Francisco: ASP), 71
- Stockman, H. S., Schmidt, G. D., Berriman, G., Liebert, J., Moore, R. L., & Wickramasinghe, D. T. 1992, *ApJ*, 401, 628
- Szkody, P., & Brownlee, D. E. 1977, *ApJ*, 212, L113
- Tovmassian, G., et al. 1999, in ASP Conf. Ser. 157, Annapolis Workshop on Magnetic Cataclysmic Variables, ed. C. Hellier & K. Mukai (San Francisco: ASP), 133
- Warner, B. 1995, *Cataclysmic Variable Stars* (Cambridge: Cambridge Univ. Press)
- Wickramasinghe, D. T., & Meggitt, S. M. A. 1985, *MNRAS*, 214, 605
- Zickgraf, F.-J., et al. 1997, *A&AS*, 123, 103